CHEMISTRY OF MATERIALS

pubs.acs.org/cm

Perspective

Ferroelectric Domains and Domain Walls in Organic–Inorganic Hybrid Perovskites

Published as part of Chemistry of Materials special issue "Chemistry of Emergent 2D Materials".

Yixin Li, Yuanyuan Jin, and Kai Leng*

Cite This: https://doi.org/10.1021/acs.chemmater.5c01042

Read Online

ACCESS | Metrics & More | Article Recommendations

ABSTRACT: Ferroelectric domains and domain walls (DWs) in organic–inorganic hybrid perovskites (OIHPs), particularly in 2D OIHPs, represent an intriguing platform for studying how unique microscopic properties can emerge at the domain level that are distinct from bulk properties. Ferroelectric domains and DWs feature domain-specific chiral photonics, charge separation pathways, nonlinear optical responses, and a domain-switchable spin texture. The relative orientations of differently polarized ferroelectric domains can break mirror symmetries and generate planar chirality, leading to metasurface-like responses toward light. The ability to reverse spin textures under an electric field offers dynamic control over spin states, making them highly suitable for spintronic applications. Recent advances in atomic-scale characterization have provided valuable insights into the atomic arrangements within ferroelectric domains and DWs that are different from ferroelastic domains in 2D OIHPs. The ability to produce a specific domain structure and control their polarization unlocks a materials platform where chirality, spin, charge, and light are dynamically coupled. This convergence could redefine optoelectronics, spintronics, and energy technologies, paving the way for a transformative future of adaptive multifunctional devices.

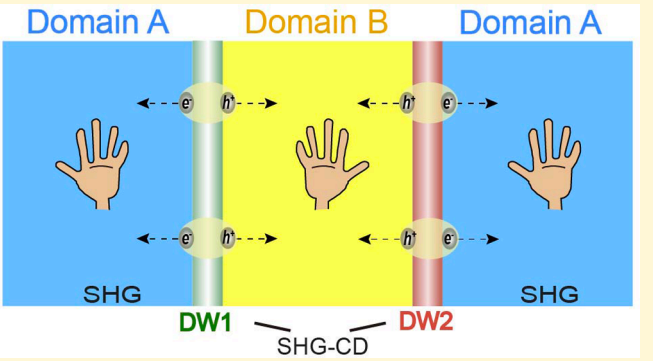

INTRODUCTION

Perovskite ferroelectrics, evolving from inorganic oxides to organic–inorganic hybrid and all-organic variants with tunable dimensionalities, demonstrate versatile functionalities for applications in photovoltaics, memory, sensors, and optoelectronics.[1−4] Recent advances highlight microscale ferroelectric domains in 2D OIHPs as a platform, offering exciting prospects for chiral photonics, spin texture, and metasurface-like elements capable of tailoring optoelectronic properties, diverging from conventional bulk-centric studies.[5,6] These domains enable precise control over symmetry-breaking effects and interfacial phenomena, which is critical for advancing device miniaturization. This perspective reviews the optical properties of ferroelectric domains, atomic-scale polarization dynamics, and domain-switchable spin texture, with a view toward designing next-generation electrically switchable chiro-optical and spintronic devices.

Ferroelectric domains in OIHPs drive emergent optoelectronic functionalities through nanoscale polarization and multicomponent coupling (lattice, charge, spin, light).[7−10] These domains enhance photovoltaic efficiency by generating internal fields that promote charge separation, while DWs—acting as nanoscale interfaces—exhibit a typical properties like localized conductivity and tunable optical absorption.[11,12] Such features stem from symmetry-breaking effects and bound charges absent in the bulk. The interplay of polarization with spin and charge enables quantum phenomena (e.g., Rashba splitting, topological states), opening pathways for spintronics and quantum computing.[13−15] Light–domain interactions further yield dynamic responses, including photoinduced polarization switching and nonlinear optical effects, which could underpin reconfigurable photonic devices. This perspective examines the ferroelectric domains in OIHPs and explores their domain-specific optoelectronic behaviors and atomic-scale characterization, highlighting their potential applications as spin-based optoelectronics as well as metasurfaces.[5] Future progress will depend on unraveling domain-driven quantum effects and achieving scalable integration into functional devices.

Received: April 29, 2025
Revised: June 23, 2025
Accepted: July 1, 2025

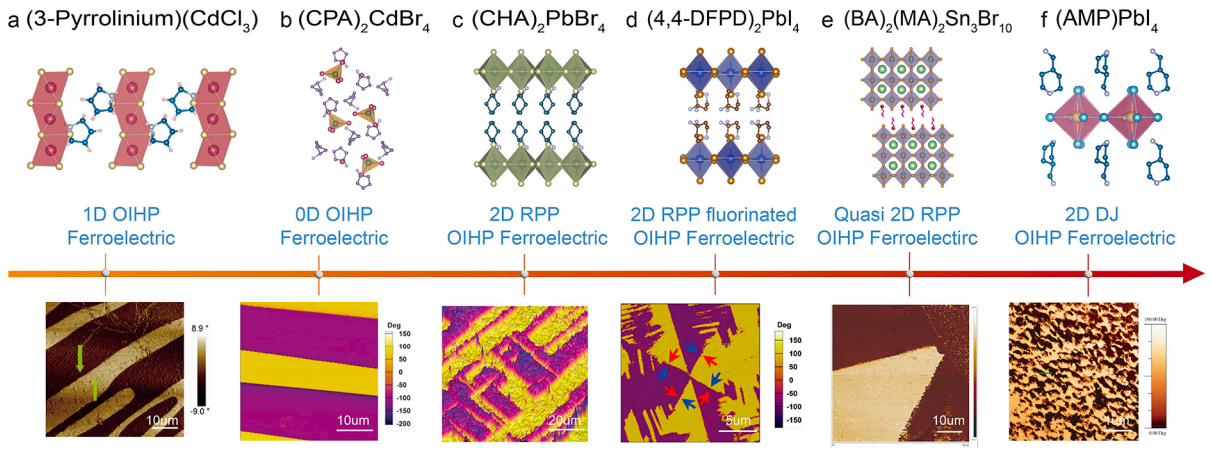

Figure 1. Ferroelectric domains with different geometric orientations in OIHPs of various dimensionalities. (a) 1D OIHP (3-Pyrrolinium)$CdCl_3$ with striped ferroelectric domains. Adapted with permission from ref 21, Copyright 2014 Wiley Online Library. (b) 0D OIHP $(CPA)_2CdBr_4$ with striped ferroelectric domains. Adapted from ref 23, Copyright 2020 American Chemical Society. (c) 2D RP phase OIHP $(CHA)_2PbBr_4$ with grid-like ferroelectric domains. Adapted with permission from ref 24, Copyright 2016 Wiley Online Library. (d) 2D RP phase of OIHP $(4,4\text{-}DFPD)_2PbI_4$ with vortex-like ferroelectric domains. Adapted from ref 25, Copyright 2020 American Chemical Society. (e) Quasi-2D RP phase OIHP $(BA)_2(MA)_3Sn_4Br_{10}$ with strip-like ferroelectric domains. Adapted from ref 26, Copyright 2020 American Chemical Society. (f) 2D DJ phase OIHP $(AMP)PbI_4$ with amorphous ferroelectric domains. Adapted from ref 27, Copyright 2019 American Chemical Society.

EVOLUTION OF OIHP FERROELECTRICS WITH FERROELECTRIC DOMAINS

Since this perspective focuses on hybrid perovskites, we will omit the discussion of inorganic perovskite ferroelectrics, which have already been extensively studied. Instead, we concentrate on the unique ferroelectric mechanisms and domain phenomena within hybrid perovskite systems. In OIHPs, the most widely accepted mechanism for ferroelectricity arises from the synergistic effect of the displacement of ions within the inorganic cage (octahedron) and the ordering of organic cations.[16,17] In improper ferroelectric OIHPs, ferroelectricity results from complex couplings between multiple order parameters—such as structural distortions, magnetic ordering, or charge density waves—with polarization being a secondary effect. Ferroelectric domains in hybrid perovskites are regions in which the polarization is uniformly aligned in the same direction. These domains form to mitigate the electrical instability that arises when the polarization is aligned uniformly throughout the material. Ferroelectric domains in OIHPs were initially studied in 3D methylammonium lead iodide ($MAPbI_3$).[18] However, whether 3D hybrid perovskites exhibit intrinsic ferroelectricity remains a topic of ongoing debate due to the centrosymmetric crystal structure. Some studies propose that the observed pseudoferroelectricity in $MAPbI_3$ can be attributed to the alignment or dynamic reorientation of methylammonium (MA^+) ions rather than true bulk ferroelectricity.[19,20] Following the investigations into 3D hybrid perovskites, ferroelectric domains have also been reported in 1D hybrid perovskites, such as (3-Pyrrolinium)-$[CdCl_3]$ (Figure 1a).[21] This material exhibits antiparallel 180° domains, which are associated with its anomalous photovoltaic properties. Recently, a large spontaneous polarization (P_s) of 24.14 $\mu C/cm^2$, along with strong second harmonic generation (SHG), was observed in the ferroelectric domains of the 1D hybrid perovskite $DMAGeI_3$ (DMA = Dimethylamine).[22] The occurrence of ferroelectric domains is due to self-organization into distinct geometric arrangements to minimize electrostatic and elastic energy. In striped domains, alternating polarization regions form parallel stripes, which are often observed in thin films or under confinement. These also encompass 0D hybrid perovskite, $[cyclopentylammonium]_2CdBr_4$ (Figure 1b), which are stabilized by competition between depolarization fields and domain-wall energy.[23] The polarization vectors in adjacent domains can be antiparallel. These are common due to low energy costs for polarization reversal. Grid-like patterns in 2D Ruddlesden−Popper perovskites (RPPs) like $n = 1$ $(CHA)_2PbBr_4$ (Figure 1c), where polarization alternates in orthogonal directions form "twin domains", minimizing long-range strain.[24] We will highlight that such orthogonally polarized domains in fact offer metasurface-like properties and can change the polarization of light. By careful design, vortex/antivortex domains consisting of spiral arrangements of polarization is also possible in $n = 1$ RPP $(4,4\text{-}DFPD)_2PbI_4$, driven by competing interactions (e.g., dipolar vs elastic forces).[25] As shown in Figure 1d, it revealed vortex-like ferroelectric domains with flux-closure patterns alongside 90° and 180° configurations, indicating that external electric fields can modulate topological domain states—a key insight for controlled domain engineering in 2D OIHPs. Such vortex/antivortex domains are promising for topological photonics and memory.

Compared to their $n = 1$ counterparts, $n > 1$ RPP ferroelectrics exemplified by $(BA)_2(MA)_2Sn_3Br_{10}$ (Figure 1e) offer enhanced practicality for functional devices due to their quasi 2D structure.[26] Reduced structural symmetry in these systems strengthens the coupling between ferroelectricity and Rashba band splitting while boosting nonlinear optical performance, positioning them as promising candidates for advanced optoelectronics. Furthermore, $n > 1$ RPP ferroelectrics also alleviates the large band gap limitations inherent to $n = 1$ analogs, a critical factor for electronic device applications. 2D Dion-Jacobson (DJ) phase perovskites, such as $(AMP)PbI_4$ (Figure 1f), also exhibit ferroelectricity.[27] One notable advantage of DJ phase perovskites is their out-of-plane ferroelectric polarization, as opposed to the in-plane polarization observed in RP phase ferroelectrics.[28] However, the ferroelectric domains reported in DJ phases thus far are randomly ordered, as shown in Figure 1f. This randomness arises from the difficulty in isolating single-crystalline DJ

https://doi.org/10.1021/acs.chemmater.5c01042
Chem. Mater. XXXX, XXX, XXX−XXX

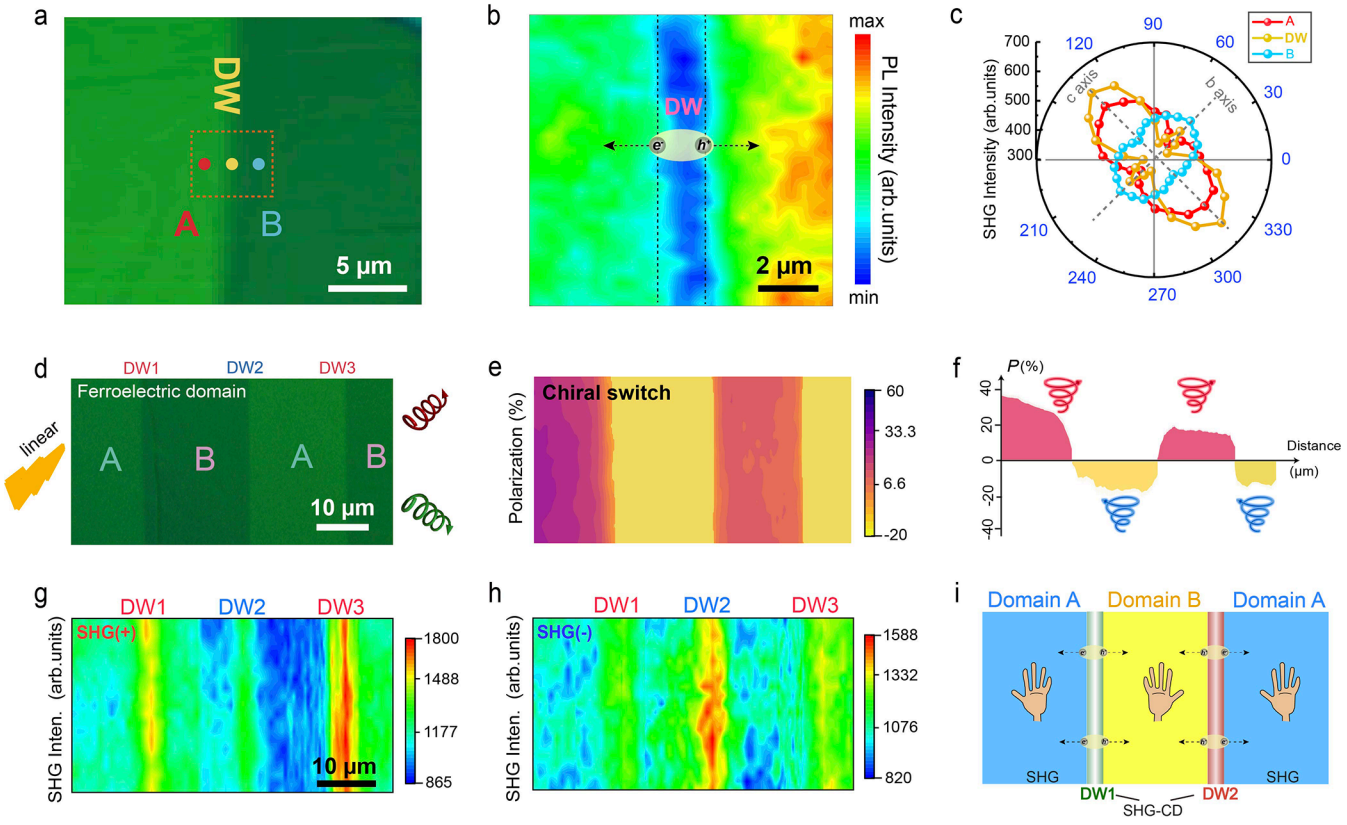

Figure 2. Domain and DW-specific optical properties in 2D OIHP ferroelectrics. (a) POM image of single-crystalline ferroelectric domain A and B, along with a DW in $(BA)_2(MA)Pb_2Br_7$. (b) PL intensity mapping of the domain A, B and DW, revealing carrier separation occurring at the DW. (c) Polarization-resolved SHG intensity on the domain A, B and DW. (d) Sequential ferroelectric domains A−B−A−B excited under linear polarized light, exhibiting chiral PL emission. (e) Circular polarization mapping of the A−B−A−B domains, demonstrating chiral switching. (f) Polarization degree values across the A−B−A−B domains. (g) SHG-CD mapping of (d) under right-handed circularly polarized light (+) detection. (h) SHG-CD mapping of (d) under left-handed polarized light (−) detection. Adapted from ref 5, available under a CC-BY 4.0. Copyright 2024 Springer Nature. (i) Schematic illustration summarizing domain and DW-specific optical properties.

ferroelectrics with the desired thickness due to their significantly stronger interlayer bonding compared to RPPs. Overcoming this limitation requires the development of advanced growth techniques, such as molecular beam epitaxy and chemical vapor deposition, to grow DJ perovskite films with precise thicknesses optimized for practical applications..

OPTOELECTRONIC PROPERTIES OF FERROELECTRIC DOMAINS IN OIHPS

Recent studies have identified highly ordered ferroelectric domains in single-crystalline 2D RPPs with higher n values, such as $(BA)_2(MA)Pb_2Br_7$ (n = 2) and $(BA)_2(MA)_2Pb_3Br_{10}$ (n = 3). These materials serve as promising platforms for investigating domain-specific optoelectronic properties. Polarized optical microscopy (POM) images reveal distinct striped adjacent domains in $(BA)_2(MA)Pb_2Br_7$, along with a DW (Figure 2a), while photoluminescence (PL) mapping shows suppressed emission at DWs.[5] This suppression stems from photoexcited electron−hole pairs migrating to opposing sides of charged DWs (Figure 2b), confirming that ferroelectric DWs in 2D OIHPs facilitate efficient charge separation—a critical feature for photovoltaic and photodetector applications, distinguishing them from ferroelastic domains. Domain-engineered structures could enhance SHG or parametric amplification. Electric control over domain arrangements might enable real-time tuning of nonlinear coefficients, which is useful in on-chip photonic circuits for signal processing or quantum light sources. SHG signals, intrinsic to non-centrosymmetric ferroelectric phases, are notably amplified at DWs. This enhancement arises from localized electric fields generated by polarization mismatches across adjacent domains. In $(BA)_2(MA)Pb_2Br_7$, polarized SHG measurements reveal a 90° phase shift between neighboring domains, with DWs exhibiting stronger SHG signals than the lower-symmetry domains themselves (Figure 2c). Structurally, 2D RPPs primarily display in-plane ferroelectricity, aligning with anisotropic charge transport along their metal halide layers. In contrast, DJ OIHPs exhibit out-of-plane ferroelectric polarization, enabling vertical charge migration across inorganic layers—an essential trait for optoelectronic devices with vertical architectures. For instance, non-ferroelectric DJ perovskites like $BDA_2Pb_3I_{10}$ (BDA = butane-1,4-diammonium) recently have been utilized in high-performance artificial synaptic memristors, leveraging uniform ion migration and efficient charge transport.[29] Integrating ferroelectric DJ perovskites with their inherent vertical charge separation and storage capabilities could further advance such devices by enhancing performance metrics.

The orthogonal arrangement of ferroelectric domains—where adjacent domains exhibit polarization vectors oriented at 90°—creates planar chirality by breaking in-plane mirror symmetry. Unlike molecular chirality, which involves the introduction of chiral molecules, planar chirality arises from the spatial arrangement of components in a planar or quasi-

https://doi.org/10.1021/acs.chemmater.5c01042
Chem. Mater. XXXX, XXX, XXX−XXX

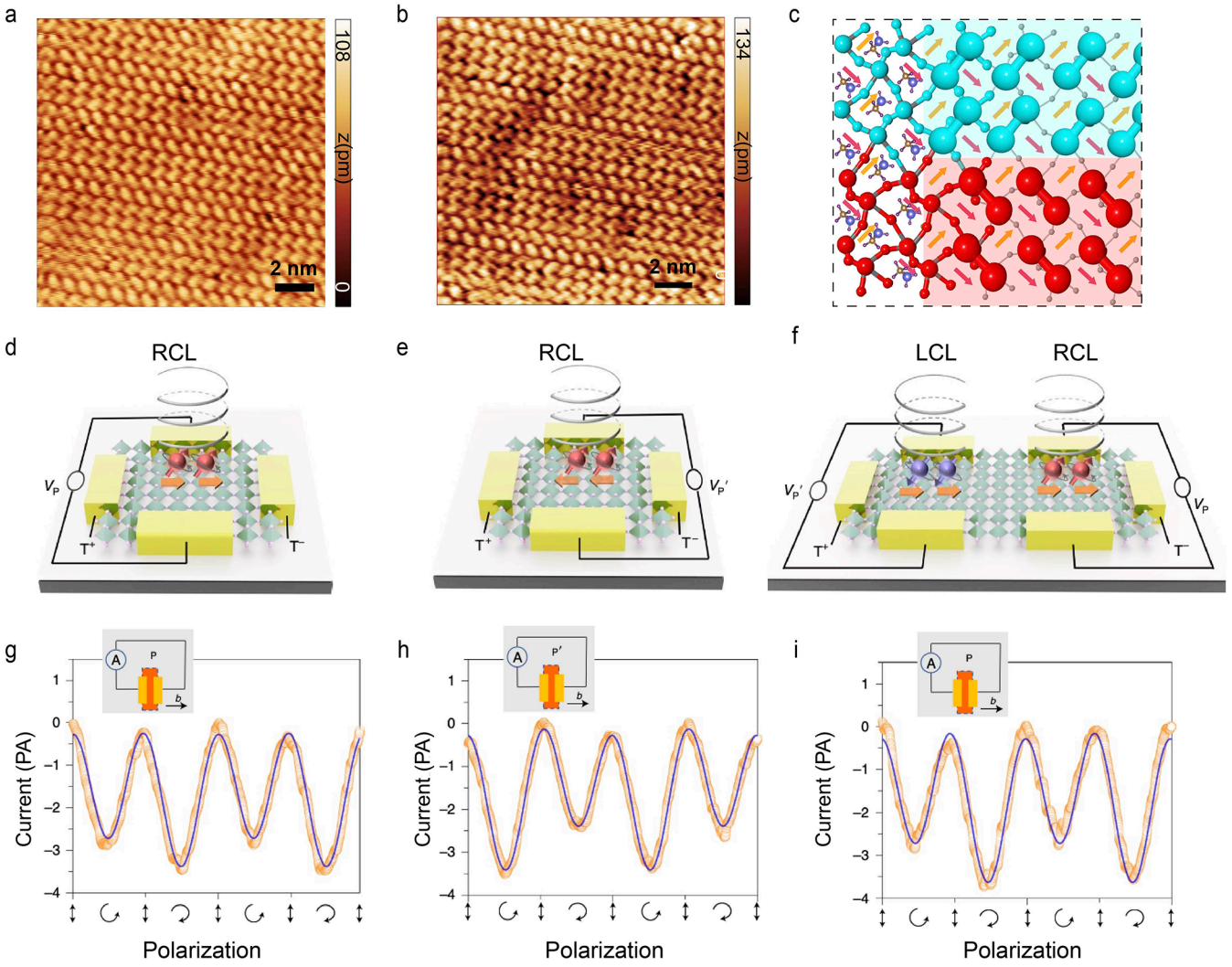

Figure 3. Atomic imaging of 2D OIHP $(BA)_2(MA)_2Pb_3Br_{10}$ ferroelectric and ferroelectrically switchable persistent spin texture in 2D OIHP (4,4-DFPD)$_2PbI_4$ ferroelectric. (a) Atomic configuration of the ferroelectric domain in $(BA)_2(MA)_2Pb_3Br_{10}$, showcasing a double Br-dimer row structure by ncAFM imaging. (b) Br-dimer row patterns, arranged in either triple or double configurations as indicated by blue and red rectangles, respectively, demonstrating the breaking of surface mirror symmetry. (c) Schematic representation of the double Br-dimer row patterns, where each blue or red dot represents a Br atom. The alignment of inner MA^+ dipoles illustrates the polarization orientation. Adapted from ref 5, available under a CC-BY 4.0. Copyright 2024 Springer Nature. (d,e) Device demonstration of spin-down electron transport direction reversal by applying an electric field along either the P_s polarization or P_s' polarization direction in (4,4-DFPD)$_2PbI_4$ under right circularly polarized light (σ^+) excitation. (f) Device demonstration of spin state manipulation via ferroelectric domains corresponding to P_s and P_s' in a single device. (g–i) Repeatedly electrically switchable circular photogalvanic effect measurements following the polarization sequence of P_s (g) → P_s' (h) → P_s' (i) by continuously alternating between σ^+ and σ^- excitation. Adapted with permission from ref 38, Copyright 2022 Springer Nature.

planar configuration, rendering the structure and its mirror image nonsuperimposable. Achiral 2D OIHPs with highly ordered ferroelectric domains exhibiting orthogonal polarization can display a planar chirality. Notably, this occurs even though the overall structure, when averaged across all domains, remains achiral. Planar chirality can be experimentally probed via polarization-dependent SHG, as chiral arrangements modify symmetry-governed nonlinear optical responses, and it enables applications in chiral optoelectronics, including circularly polarized light detection.[30] Planar chirality has recently been reported in the highly ordered ferroelectric domains of $(BA)_2(MA)Pb_2Br_7$ (n = 2) and $(BA)_2(MA)_2Pb_3Br_{10}$ (n = 3) despite the bulk crystal itself being achiral. As illustrated in Figure 2d, under linear light excitation, ferroelectric domains with A−B−A−B patterns can exhibit left-handed (L.H.)−right-handed (R.H.)−L.H.−R.H. circularly polarized light emission, demonstrating domain-switchable chirality (Figure 2e). The polarization P ((R.H. PL − L.H. PL)/(R.H. PL + L.H. PL)), which reflects the circular dichroism (CD) effect, shows the following values: domain A exhibits P_+ = 37.5%, while domain B shows P_- = 20.3% (Figure 2f), values that are comparable to those observed in chiral molecule-induced OIHPs. In addition, as shown in Figure 2g, h, a strong SHG-CD response is observed at the DWs. The handedness of the circularly polarized SHG signal switches between adjacent DWs due to the reversed ferroelectric polarization, further highlighting the chiral optical behavior of these ferroelectric DWs.[31] An impressive SHG-CD anisotropy factor ($g_{SHG\text{-}CD}$) of 0.41 has been reported at the DWs compared with domains, reflecting strong chiroptical sensitivity and contrast. The planar chiral optical phenomena discussed above, observed in both the domains and the DWs of

https://doi.org/10.1021/acs.chemmater.5c01042
Chem. Mater. XXXX, XXX, XXX−XXX

2D OIHPs, are summarized and illustrated in Figure 2i. Unlike 3D chiral OIHPs, this in-plane chirality in 2D OIHPs is surface-sensitive and dynamically tunable via electric fields, offering a platform for ultrathin, reconfigurable devices where domain-engineered polarization states govern functionality. These chiral optical responses in both the 2D OIHP ferroelectric domains and DWs present an opportunity for advanced memristor device applications. By leveraging the chiral optical properties of the ferroelectric domains and DWs, it becomes possible to introduce an additional degree of freedom for data storage and processing.[32,33] Specifically, the alternating chiral states of the domains, responsive to linearly polarized light, can serve as distinct data states, such as "0" and "1". The ability to manipulate these chiral states using optical stimuli adds a novel dimension to memristor functionality, enabling multistate data storage and enhanced device performance.

ATOMIC IMAGING OF FERROELECTRIC DOMAINS IN 2D OIHPS

The ferroelectric domains that appear as parallel stripes under a microscope consist of finer features within the stripes whose arrangements reveal how the polarization axes are arranged between adjacent domains. Figure 3a, b illustrate the atomic arrangement in $(BA)_2(MA)Pb_2Br_7$. In Figure 3a, b, an elongated point represents a pair of Br atoms located at the apexes of two out-of-plane tilted $[PbBr_6]^{4-}$ octahedra, revealing a Br-dimer row structure. These Br-dimer rows appear in varying numbers—single, double, or triple—breaking the surface mirror symmetry and exhibiting a nonzero polarization. The Br-dimer row structure emerges from a delicate balance of electrostatic forces dictated by the arrangement of methylammonium ions (MA^+), as illustrated by the yellow and pink arrows in Figure 3c. Consequently, the vector addition of the yellow and pink arrows produces a net polarization direction along the b and c axes, as indicated by the purple arrows in Figure 3c. These atomic patterns lead to both the ferroelectric Rashba effect and planar chirality in the $(BA)_2(MA)Pb_2Br_7$ domains, as discussed above. In contrast to the dimer-like atomic structure of the ferroelectric domains, the DWs exhibit a square-like lattice structure. The DWs traverse two ferroelectric domains with orthogonal electric polarizations, explaining the change in atomic structure. This leads to stronger second-harmonic SHG-CD at the DWs compared to the domain regions.

DOMAIN WALLS AS HOTSPOTS FOR ENHANCED SPIN SPLITTING IN 2D OIHPS

Rashba spin splitting is a quantum phenomenon arising from the interplay between an electron's spin and its momentum in systems with broken inversion symmetry. This effect manifests as a momentum-dependent splitting of energy bands into spin-polarized states, where electrons with opposite spins (e.g., "up" and "down") occupy distinct energy levels.[34] The splitting is induced by spin−orbit coupling (SOC)—a relativistic interaction between an electron's spin and its motion in an electric field—combined with structural or electric-field-induced asymmetry. Materials exhibiting strong Rashba effects, such as Pb-based OIHPs, are particularly promising for spintronics as their spin textures can be controlled via external stimuli like electric fields.[35] This electrical tunability offers a pathway to encode and manipulate spin information without magnetic fields, a cornerstone for low-power, high-speed spin-based devices. Ferroelectric domains in 2D OIHPs with low symmetry host Rashba spin textures, where electron spin orientations are intricately linked to local polarization directions. As ferroelectric polarization can be reversed by an applied electric field, spin textures are directly influenced by the polarization, and reversing the polarization can switch the spin texture. Furthermore, adjacent domains with opposing or orthogonal polarizations exhibit distinct spin-momentum locking patterns, as the effective electric field governing SOC reverses or reorients across domain boundaries.[36,37] For instance, a domain polarized along the b direction will generate a spin texture with clockwise helicity, while its neighboring domain polarized along the c direction will display counter-clockwise helicity. This allows electrically switchable spin textures: by reorienting ferroelectric polarization, the Rashba-induced spin-splitting direction can be toggled, enabling nonvolatile control over spin currents. At DWs, interfaces separating regions with mismatched polarizations and the abrupt change in polarization as well as strain generates a steep electric field gradient. This locally amplified field intensifies Rashba splitting, creating spin-polarized channels with momentum-dependent spin orientations that deviate from those in bulk domains. The interplay between domain architecture and spin texture offers novel device-design strategies. Engineered domain wall arrays could serve as spin-waveguides or interconnects in spin-based circuits. This paradigm highlights 2D OIHP ferroelectric DWs as a versatile platform for merging ferroelectric memory and spin logic, bridging the gap between semiconductor electronics and quantum information technologies.

FERROELECTRIC POLARIZATION P_S SWITCHABLE PERSISTENT SPIN TEXTURE

Based on the C_{2v} point group symmetry of 2D OIHP $(4,4\text{-DFPD})_2PbI_4$, where 4,4-DFPD refers to 4,4-difluoropiperidinium, it has been suggested that it has symmetry-enforced persistent spin texture (PST), where the spin orientation of electrons remains locked to their momentum over extended timescales.[38] PST arises from the uniaxial symmetry of the crystal, which suppresses spin relaxation mechanisms (e.g., Dyakonov−Perel scattering). This stability is critical for maintaining spin coherence in the devices. The ferroelectric nature in $(4,4\text{-DFPD})_2PbI_4$ enables polarization reversal by electrical switching. For example, the spin-up band in the $+k_y$ direction near the conduction band minimum (CBM) can be switched to the spin-down band simply by electrically poling the crystal polarization from the +a direction to the −a direction. The electrically switchable nature of PST has also been theoretically verified in another ferroelectric 2D OIHP, $(PA)_2CsPb_2Br_7$, by reversing the direction of its ferroelectric polarization (P_s).[6] However, experimental validation of PST switching remains challenging. One approach to experimentally test ferroelectrically switchable PST is by utilizing circular photogalvanic effect (CPGE). As illustrated in Figure 3d, e, by applying an external electrode either along the material's P_s polarized state or reversed P_s' state under right circularly polarized light ($\sigma+$) excitation, the spin-down electron transport direction is reversed, as indicated by the orange arrows pointing to the right/left directions. By continuously alternating between σ^+ and σ^- excitations, a reversible and cyclic photogalvanic effect is observed, following the sequence $P_s \rightarrow P_s' \rightarrow P_s$ (Figure 3g–i). If the material exhibits

https://doi.org/10.1021/acs.chemmater.5c01042
Chem. Mater. XXXX, XXX, XXX−XXX

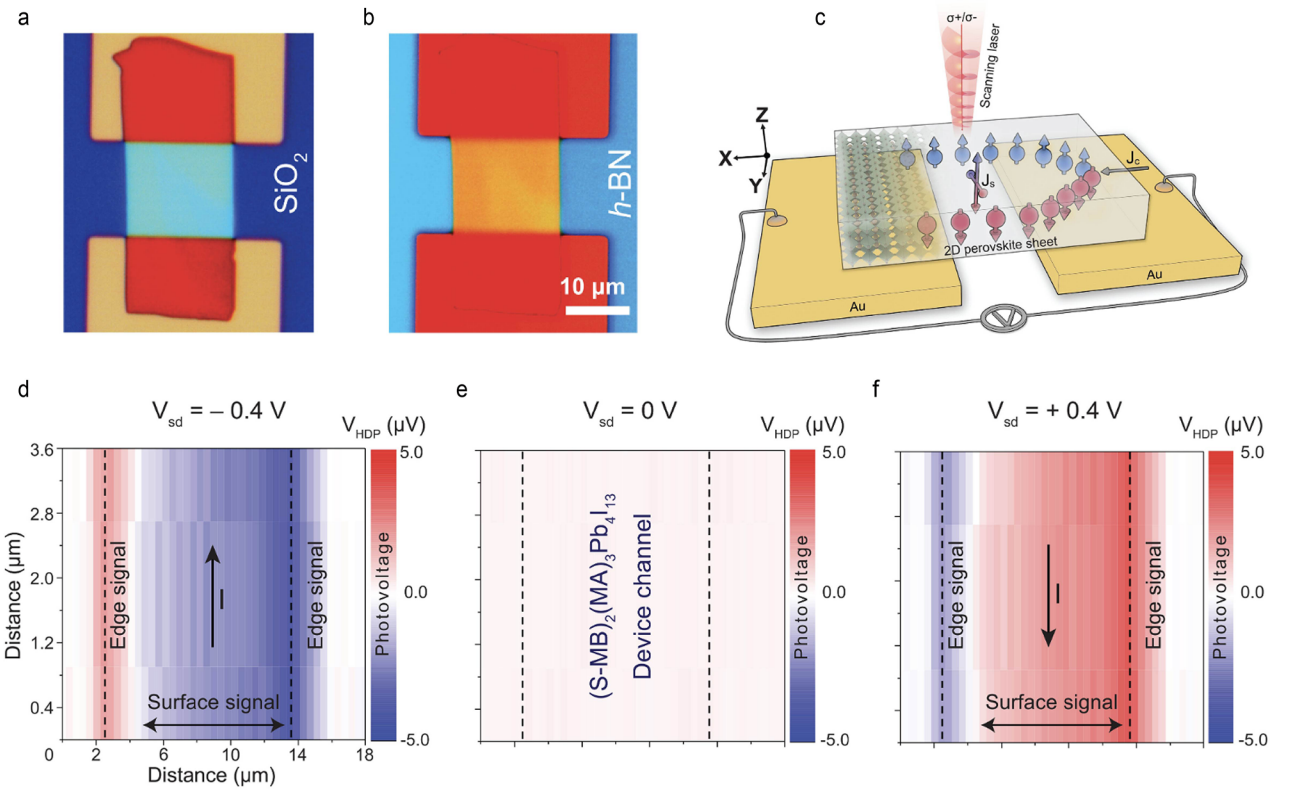

Figure 4. Charge-to-spin conversion in chiral $n = 4$ 2D OIHP $(R/S\text{-}MBA)_2(MA)_3Pb_4I_{13}$. (a) Optical image of a Hall bar-like device constructed on sharp-edged, single-crystalline $(R/S\text{-}MBA)_2(MA)_3Pb_4I_{13}$ thin film. (b) Encapsulation of the device with an h-BN protection layer. (c) Schematic illustration of a transverse spin current generated via the spin Hall effect. (d–f) Spatially resolved scanning helicity-dependent photovoltage maps under reverse and zero bias voltages of (d) $V_{sd} = -0.4$ V, (e) $V_{sd} = 0$ V, and (f) $V_{sd} = +0.4$ V. Blue and red colors represent spin-up and spin-down signals, respectively. Adapted with permission from ref 40, Copyright 2024 AAAS.

ferroelectric domains with alternating P_s and P_s' polarizations in adjacent domains, the spin states can be manipulated through the corresponding ferroelectric domains within a single device, as shown in Figure 3f. Another direct way to confirm PST is to map the diffusive evolution of a local spin excitation into a helical spin mode by a time- and spatially resolved magneto-optical Kerr rotation technique.[39] Bridging this theory–experiment gap requires advanced characterization techniques, such as spin-resolved angle-resolved photoemission spectroscopy (spin-ARPES), to directly map the spin texture before and after polarization switching. The coupling between ferroelectric polarization and spin texture—termed "ferroelectrically tunable Rashba splitting—suggests that 2D OIHP ferroelectrics could serve as reconfigurable spin filters or memory elements in spintronic circuits.

CHIRAL 2D PEROVSKITES: SPIN CURRENTS BEYOND CONVENTIONAL SYMMETRY

In chiral 2D OIHPs, the chirality is transferred from organic chiral cations to the inorganic sublattices, reducing the bulk symmetry of the crystal and introducing Rashba–Dresselhaus SOC. Moreover, chiral materials can enable spin-selective electron transport through the chiral-induced spin selectivity effect. Recent experiments on chiral 2D OIHPs, such as $n = 4$ $(R/S\text{-}MBA)_2(MA)_3Pb_4I_{13}$ (where MBA refers to R/S-methylbenzylammonium), have broadened the possibilities for spin control in perovskites.[40] In $(R/S\text{-}MBA)_2(MA)_3Pb_4I_{13}$, chirality is transferred from the organic R/S-MBA cations to the inorganic framework, breaking mirror symmetries and enabling unconventional spin-to-charge interconversion. As illustrated in Figure 4a, b, single-crystalline exfoliated thin films of $(R/S\text{-}MBA)_2(MA)_3Pb_4I_{13}$ ($n = 4$), featuring sharp edges, were used to construct a Hall bar device with a protective layer. In this device, an applied charge current generates a transverse spin current via the spin Hall effect (Figure 4c), characterized by a spin Hall angle (θ_{sh}) of 5% (the ratio of spin current density to charge current density) and a spin lifetime (τ_s) of approximately 75 ps at room temperature. The τs of the $n = 4$ RPPs is much longer than those of heavy metals (Pt, 0.57 ps) and topological insulators (Bi_2Se_3, 3.3 ps) and lower-n homologues.[41,42] Scanning helicity-dependent photovoltage (HDP) maps reveal a switchable spin polarization with opposite signs upon reversing the bias current direction with spin accumulation observed along the two edges of the device (Figure 4d–f). Moreover, HDP signals are also detected in the central channel, indicating that the low symmetry of the chiral lattice generates an out-of-plane spin current, orthogonal to the conventional transverse flow. This 3D spin texture could pave the way for novel device architectures, such as vertical spin valves or multiaxis spin–orbit torque systems. Looking ahead, the development of chiral ferroelectric 2D OIHPs could further enhance the spin Hall angle, providing even greater opportunities for spintronic applications. The addition of ferroelectricity as an additional degree of freedom would open up exciting possibilities for exploring spintronic phenomena in chiral ferroelectric 2D OIHPs.

https://doi.org/10.1021/acs.chemmater.5c01042
Chem. Mater. XXXX, XXX, XXX–XXX

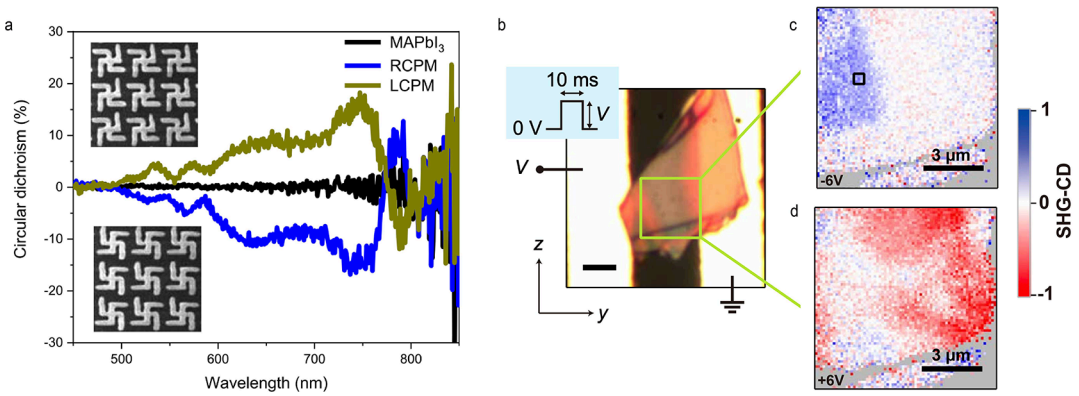

Figure 5. Metasurfaces in OIHPs. (a) Circular dichroism measurements of gammadion patterned right-handed $MAPbI_3$ chiral metasurface (RPCM), left-handed $MAPbI_3$ chiral metasurface (LPCM), and unpatterned $MAPbI_3$. Adapted with permission from ref 46, available under a CC-BY 4.0. Copyright 2024 Springer Nature. (b) Optical microscopy image of an exfoliated 2D ferroelectric $(BA)_2(EA)_2Pb_3I_{10}$ on electrodes. (c,d) Electrically switchable nonlinear chiroptical SHG-CD responses, mapped at voltages of $V = -6$ V (c) and $V = +6$ V (d) Adapted with permission from ref 47, available under a CC-BY 4.0. Copyright 2024 AAAS.

2D OIHP FERROELECTRICS: PROMISING CANDIDATES FOR METAMATERIALS

Metasurfaces are 2D arrays of subwavelength nanostructures that control light at the nanoscale. They enable tailored interactions with electromagnetic waves, such as bending, focusing, or altering polarization, for applications in optics and photonics.[43] We can leverage the high refractive index in 2D OIHPs for strong light−matter interactions, low optical losses for efficiency, tunable bandgaps for wavelength-specific optimization, and strong light absorption. By integrating chirality (enabling polarization control) and ferroelectricity (allowing electric-field-driven reconfigurability), 2D OIHP ferroelectric-based metasurfaces can potentially enable advanced functionalities in optoelectronics, chiral photonics (e.g., polarization-sensitive devices), and nonlinear lasing. The manufacturability of OIHP metasurfaces has been demonstrated using techniques such as nanoimprinting, focused ion beam milling, and cryogenic electron-beam writing.[44−46] These fabrication methods enable the precise creation of intricate nanoscale patterns, allowing OIHP metasurfaces to manipulate light in unique and efficient ways. For instance, giant superstructural chirality with a circular dichroism value of 6350 mdeg and anisotropy factor (gCD) of 0.49 has been experimentally achieved on spin-coated, nonchiral 3D $MAPbI_3$ thin films by introducing arrays of gammadion patterns (Figure 5a).[46] Furthermore, simulations suggest that g_{CD} of 1.11 and circular dichroism value of 18,900 mdeg (theoretical limits) could be realized for these geometrical metasurface designs.

It is particularly promising to leverage the highly ordered ferroelectric domains in the OIHPs to make metasurfaces. Notably, planar chirality has already been observed in the orthogonally aligned ferroelectric domains of $(BA)_2(MA)Pb_2Br_7$, contributing to circular dichroism. When two domains are aligned orthogonally, their polarization vectors form a structural pattern without in-plane mirror symmetry. The ability to break mirror symmetry via domain orientation enables metasurface-like control over light polarization, phase, and amplitude. Electrically switching domains allows dynamic tuning of optical responses, paving the way for adaptive lenses, holographic displays, and beam-steering devices. Recent breakthroughs, such as electrically switchable chiral nonlinear optics in achiral 2D $(BA)_2(EA)_2Pb3I_{10}$ (Figure 5b−d), highlight the potential to combine metasurface engineering with external electric fields.[47] This synergy could enable dynamic, reversible control over circular polarization states—critical for advancing spintronics, quantum information processing, and tunable chiral light sources. Applying metasurface patterning on 2D ferroelectric OIHPs can enhance the g_{CD} values significantly, while their intrinsic nonlinear multiphoton emission enables metasurface-controlled photonic Rashba effects for tunable upconversion PL.

In conclusion, the study of ferroelectric domains and DWs in 2D OIHPs has revealed a wealth of opportunities for advancing reconfigurable optical metasurfaces and domain wall electronics. The ability of ferroelectric domains to enhance photovoltaic efficiency, enable Rashba spin splitting, and provide metasurface-like control over light's polarization suggests that their integration with advanced metasurface designs could further expand their application potential. For instance, metasurfaces patterned with alternating domain polarities can function as nonlinear photonic crystals, enabling quasi-phase-matching for efficient parametric upconversion across broad bandwidths. Despite their promise, several challenges remain including controlled growth of ferroelectric domains, ensuring domain stability during repeated switching, achieving scalable domain patterning, and integrating these materials with existing semiconductor nanotechnology. Addressing these challenges will require a deeper understanding of atomic-scale domain dynamics and interfacial interactions in 2D OIHP ferroelectrics, which is critical for unlocking their full potential.

AUTHOR INFORMATION

Corresponding Author

Kai Leng − *Department of Applied Physics, The Hong Kong Polytechnic University, Kowloon 999077 Hong Kong, China;* orcid.org/0000-0003-3408-5033; Email: kathy-kai.leng@polyu.edu.hk

Authors

Yixin Li − *Department of Applied Physics, The Hong Kong Polytechnic University, Kowloon 999077 Hong Kong, China;* orcid.org/0009-0008-8331-2531

Yuanyuan Jin − *Department of Applied Physics, The Hong Kong Polytechnic University, Kowloon 999077 Hong Kong, China*

https://doi.org/10.1021/acs.chemmater.5c01042
Chem. Mater. XXXX, XXX, XXX−XXX

Complete contact information is available at:
https://pubs.acs.org/10.1021/acs.chemmater.5c01042

Author Contributions

The manuscript was written through contributions of all authors. All authors have given approval to the final version of the manuscript.

Notes

The authors declare no competing financial interest.

Biographies

Kai Leng is the Associate Professor in the Department of Applied Physics at The Hong Kong Polytechnic University. She leads a research group dedicated to advancing the emerging field of molecularly thin hybrid perovskites. Her work focuses on key areas such as the isolation of these materials, precise establishment of their atomic structure−property relationships, large-area growth techniques, and the development of innovative device applications, particularly in opto-microelectronics and spintronics. She is a recipient of the MIT Technology Review Innovators Under 35-Asia Pacific Award, the Asian Young Scientist Fellowship, the Croucher Tak Wah Mak Innovation Award, the Early Career Research Gold Award from the Singapore National Institute of Chemistry, and the China Excellent Young Scientist Award.

Li Yixin is currently a PhD candidate in the Department of Applied Physics at The Hong Kong Polytechnic University. Her research focuses on the chemical vapor deposition (CVD) growth of two-dimensional hybrid perovskite single-crystalline films and the investigation of their ferroelectric properties. She specializes in the growth control, structural characterization, and ferroelectric performance analysis of low-dimensional perovskite systems for potential applications in electronic and optoelectronic devices.

Jin Yuanyuan received her PhD degree from Hunan University and is currently a postdoctoral researcher in the Department of Applied Physics at The Hong Kong Polytechnic University. Her research interests include the chemical vapor deposition (CVD) growth of two-dimensional materials, such as transition metal dichalcogenides (TMDs) and hybrid perovskites, as well as the fabrication and characterization of electronic devices based on these materials.

■ ACKNOWLEDGMENTS

K.L. acknowledges funding from Project 62322413 supported by the National Natural Science Foundation of China and the Croucher Foundation (Croucher Tak Wah Mak Innovation fund 2023) and the Research Grants Council of the Hong Kong Special Administrative Region, China (Project No. PolyU15306724).

■ REFERENCES

(1) Saparov, B.; Mitzi, D. B. Organic−Inorganic Perovskites: Structural Versatility for Functional Materials Design. *Chem. Rev.* **2016**, *116* (7), 4558−4596.
(2) Zhang, L.; Mei, L.; Wang, K.; Lv, Y.; Zhang, S.; Lian, Y.; Liu, X.; Ma, Z.; Xiao, G.; Liu, Q.; Zhai, S.; Zhang, S.; Liu, G.; Yuan, L.; Guo, B.; Chen, Z.; Wei, K.; Liu, A.; Yue, S.; Niu, G.; Pan, X.; Sun, J.; Hua, Y.; Wu, W.-Q.; Di, D.; Zhao, B.; Tian, J.; Wang, Z.; Yang, Y.; Chu, L.; Yuan, M.; Zeng, H.; Yip, H.-L.; Yan, K.; Xu, W.; Zhu, L.; Zhang, W.; Xing, G.; Gao, F.; Ding, L. Advances in the Application of Perovskite Materials. *Nano-Micro Lett.* **2023**, *15* (1), 177.
(3) Wei, H.; Fang, Y.; Mulligan, P.; Chuirazzi, W.; Fang, H.-H.; Wang, C.; Ecker, B. R.; Gao, Y.; Loi, M. A.; Cao, L.; Huang, J. Sensitive X-Ray Detectors Made of Methylammonium Lead Tribromide Perovskite Single Crystals. *Nat. Photonics* **2016**, *10* (5), 333−339.
(4) Gu, C.; Lee, J.-S. Flexible Hybrid Organic−Inorganic Perovskite Memory. *ACS Nano* **2016**, *10* (5), 5413−5418.
(5) Li, C.; Telychko, M.; Zheng, Y.; Yuan, S.; Wu, Z.; Wong, W. P. D.; Li, Y.; Jin, Y.; Io, W. F.; Wang, X.; Lin, J.; Hao, J.; Han, C.; Leng, K. Switchable Planar Chirality and Spin Texture in Highly Ordered Ferroelectric Hybrid Perovskite Domains. *Nat. Commun.* **2024**, *15* (1), 10221.
(6) Guo, W.; Xu, H.; Ma, Y.; Liu, Y.; Gao, H.; Hu, T.; Ren, W.; Luo, J.; Sun, Z. Electrically Switchable Persistent Spin Texture in a Two-Dimensional Hybrid Perovskite Ferroelectric. *Angew. Chem., Int. Ed.* **2023**, *62* (17), No. e202300028.
(7) Howard, J. M.; Lahoti, R.; Leite, M. S. Imaging Metal Halide Perovskites Material and Properties at the Nanoscale. *Adv. Energy Mater.* **2020**, *10* (26), 1903161.
(8) Gao, Y.; Walters, G.; Qin, Y.; Chen, B.; Min, Y.; Seifitokaldani, A.; Sun, B.; Todorovic, P.; Saidaminov, M. I.; Lough, A.; Tongay, S.; Hoogland, S.; Sargent, E. H. Electro-Optic Modulation in Hybrid Metal Halide Perovskites. *Adv. Mater.* **2019**, *31* (16), 1808336.
(9) Zhai, Y.; Baniya, S.; Zhang, C.; Li, J.; Haney, P.; Sheng, C.-X.; Ehrenfreund, E.; Vardeny, Z. V. Giant Rashba Splitting in 2D Organic-Inorganic Halide Perovskites Measured by Transient Spectroscopies. *Sci. Adv.* **2017**, *3* (7), No. e1700704.
(10) Pecchia, A.; Gentilini, D.; Rossi, D.; Auf Der Maur, M.; Di Carlo, A. Role of Ferroelectric Nanodomains in the Transport Properties of Perovskite Solar Cells. *Nano Lett.* **2016**, *16* (2), 988−992.
(11) Rashkeev, S. N.; El-Mellouhi, F.; Kais, S.; Alharbi, F. H. Domain Walls Conductivity in Hybrid Organometallic Perovskites and Their Essential Role in CH3NH3PbI3 Solar Cell High Performance. *Sci. Rep.* **2015**, *5* (1), 11467.
(12) Liu, S.; Zheng, F.; Koocher, N. Z.; Takenaka, H.; Wang, F.; Rappe, A. M. Ferroelectric Domain Wall Induced Band Gap Reduction and Charge Separation in Organometal Halide Perovskites. *J. Phys. Chem. Lett.* **2015**, *6* (4), 693−699.
(13) Kim, M.; Im, J.; Freeman, A. J.; Ihm, J.; Jin, H. Switchable S = 1/2 and J = 1/2 Rashba Bands in Ferroelectric Halide Perovskites. *Proc. Natl. Acad. Sci. U.S.A.* **2014**, *111* (19), 6900−6904.
(14) Kepenekian, M.; Even, J. Rashba and Dresselhaus Couplings in Halide Perovskites: Accomplishments and Opportunities for Spintronics and Spin−Orbitronics. *J. Phys. Chem. Lett.* **2017**, *8* (14), 3362−3370.
(15) Li, X.; Zhang, S.; Zhang, X.; Vardeny, Z. V.; Liu, F. Topological Nodal-Point Superconductivity in Two-Dimensional Ferroelectric Hybrid Perovskites. *Nano Lett.* **2024**, *24* (9), 2705−2711.
(16) Shahrokhi, S.; Gao, W.; Wang, Y.; Anandan, P. R.; Rahaman, M. Z.; Singh, S.; Wang, D.; Cazorla, C.; Yuan, G.; Liu, J.; Wu, T. Emergence of Ferroelectricity in Halide Perovskites. *Small Methods* **2020**, *4* (8), 2000149.
(17) Zheng, W.; Wang, X.; Zhang, X.; Chen, B.; Suo, H.; Xing, Z.; Wang, Y.; Wei, H.; Chen, J.; Guo, Y.; Wang, F. Emerging Halide Perovskite Ferroelectrics. *Adv. Mater.* **2023**, *35* (21), 2205410.
(18) Kutes, Y.; Ye, L.; Zhou, Y.; Pang, S.; Huey, B. D.; Padture, N. P. Direct Observation of Ferroelectric Domains in Solution-Processed $CH_3NH_3PbI_3$ Perovskite Thin Films. *J. Phys. Chem. Lett.* **2014**, *5* (19), 3335−3339.
(19) Leguy, A. M. A.; Frost, J. M.; McMahon, A. P.; Sakai, V. G.; Kockelmann, W.; Law, C.; Li, X.; Foglia, F.; Walsh, A.; O'Regan, B. C.; Nelson, J.; Cabral, J. T.; Barnes, P. R. F.; et al. The Dynamics of Methylammonium Ions in Hybrid Organic−Inorganic Perovskite Solar Cells. *Nat. Commun.* **2015**, *6* (1), 7124.
(20) Frost, J. M.; Butler, K. T.; Brivio, F.; Hendon, C. H.; Van Schilfgaarde, M.; Walsh, A. Atomistic Origins of High-Performance in Hybrid Halide Perovskite Solar Cells. *Nano Lett.* **2014**, *14* (5), 2584−2590.
(21) Ye, H.; Zhang, Y.; Fu, D.; Xiong, R. An Above-Room-Temperature Ferroelectric Organo− Metal Halide Perovskite: (3-Pyrrolinium)($CdCl_3$). *Angew. Chem.* **2014**, *126* (42), 11424−11429.
(22) Ding, K.; Ye, H.; Su, C.; Xiong, Y.-A.; Du, G.; You, Y.-M.; Zhang, Z.-X.; Dong, S.; Zhang, Y.; Fu, D.-W. Superior Ferroelectricity

and Nonlinear Optical Response in a Hybrid Germanium Iodide Hexagonal Perovskite. *Nat. Commun.* **2023**, *14* (1), 2863.
(23) Huang, C.-R.; Luo, X.; Liao, W.-Q.; Tang, Y.-Y.; Xiong, R.-G. An Above-Room- Temperature Molecular Ferroelectric: [Cyclopentylammonium]$_2$CdBr$_4$. *Inorg. Chem.* **2020**, *59* (1), 829−836.
(24) Ye, H.; Liao, W.; Hu, C.; Zhang, Y.; You, Y.; Mao, J.; Li, P.; Xiong, R. Bandgap Engineering of Lead-Halide Perovskite-Type Ferroelectrics. *Adv. Mater.* **2016**, *28* (13), 2579−2586.
(25) Zhang, H.-Y.; Song, X.-J.; Chen, X.-G.; Zhang, Z.-X.; You, Y.-M.; Tang, Y.-Y.; Xiong, R.-G. Observation of Vortex Domains in a Two-Dimensional Lead Iodide Perovskite Ferroelectric. *J. Am. Chem. Soc.* **2020**, *142* (10), 4925−4931.
(26) Li, L.; Liu, X.; He, C.; Wang, S.; Ji, C.; Zhang, X.; Sun, Z.; Zhao, S.; Hong, M.; Luo, J. A Potential Sn-Based Hybrid Perovskite Ferroelectric Semiconductor. *J. Am. Chem. Soc.* **2020**, *142* (3), 1159−1163.
(27) Park, I.-H.; Zhang, Q.; Kwon, K. C.; Zhu, Z.; Yu, W.; Leng, K.; Giovanni, D.; Choi, H. S.; Abdelwahab, I.; Xu, Q.-H.; Sum, T. C.; Loh, K. P. Ferroelectricity and Rashba Effect in a Two- Dimensional Dion-Jacobson Hybrid Organic−Inorganic Perovskite. *J. Am. Chem. Soc.* **2019**, *141* (40), 15972−15976.
(28) He, W.; Yang, Y.; Li, C.; Wong, W. P. D.; Cimpoesu, F.; Toader, A. M.; Wu, Z.; Wu, X.; Lin, Z.; Xu, Q.; Leng, K.; Stroppa, A.; Loh, K. P. Near-90° Switch in the Polar Axis of Dion− Jacobson Perovskites by Halide Substitution. *J. Am. Chem. Soc.* **2023**, *145* (25), 14044−14051.
(29) Kim, S. J.; Im, I. H.; Baek, J. H.; Choi, S.; Park, S. H.; Lee, D. E.; Kim, J. Y.; Kim, S. Y.; Park, N.-G.; Lee, D.; Yang, J. J.; Jang, H. W.; et al. Linearly Programmable Two-Dimensional Halide Perovskite Memristor Arrays for Neuromorphic Computing. *Nat. Nanotechnol.* **2025**, *20* (1), 83−92.
(30) Li, M.; Fang, F.; Huang, X.; Liu, G.; Lai, Z.; Chen, Z.; Hong, J.; Chen, Y.; Wei, R.; Ning, G.-H.; Leng, K.; Shi, Y.; Tian, B. Chiral Ligand-Induced Structural Transformation of Low- Dimensional Hybrid Perovskite for Circularly Polarized Photodetection. *Chem. Mater.* **2022**, *34* (7), 2955−2962.
(31) Li, C.; Yuan, S.; Li, Y.; Wu, Z.; Jin, Y.; Loh, K. P.; Leng, K. Phonon Driven Ferroelectricity and Raman Active Modes in Hybrid Organic-Inorganic Perovskites. *Adv. Mater.* **2025**, 2419685.
(32) Long, G.; Sabatini, R.; Saidaminov, M. I.; Lakhwani, G.; Rasmita, A.; Liu, X.; Sargent, E. H.; Gao, W. Chiral-Perovskite Optoelectronics. *Nat. Rev. Mater.* **2020**, *5* (6), 423−439.
(33) Dong, Y.; Zhang, Y.; Li, X.; Feng, Y.; Zhang, H.; Xu, J. Chiral Perovskites: Promising Materials toward Next-Generation Optoelectronics. *Small* **2019**, *15* (39), 1902237.
(34) Leng, K.; Li, R.; Lau, S. P.; Loh, K. P. Ferroelectricity and Rashba Effect in 2D Organic− Inorganic Hybrid Perovskites. *Trends Chem.* **2021**, *3* (9), 716−732.
(35) Jia, F.; Hu, S.; Xu, S.; Gao, H.; Zhao, G.; Barone, P.; Stroppa, A.; Ren, W. Persistent Spin- Texture and Ferroelectric Polarization in 2D Hybrid Perovskite Benzylammonium Lead-Halide. *J. Phys. Chem. Lett.* **2020**, *11* (13), 5177−5183.
(36) Chakraborty, R.; Sercel, P. C.; Qin, X.; Mitzi, D. B.; Blum, V. Design of Two-Dimensional Hybrid Perovskites with Giant Spin Splitting and Persistent Spin Textures. *J. Am. Chem. Soc.* **2024**, *146* (50), 34811−34821.
(37) Gupta, M.; Nanda, B. R. K. Spin Texture as Polarization Fingerprint of Halide Perovskites. *Phys. Rev. B* **2022**, *105* (3), 035129.
(38) Zhang, L.; Jiang, J.; Multunas, C.; Ming, C.; Chen, Z.; Hu, Y.; Lu, Z.; Pendse, S.; Jia, R.; Chandra, M.; Sun, Y.-Y.; Lu, T.-M.; Ping, Y.; Sundararaman, R.; Shi, J. Room-Temperature Electrically Switchable Spin−Valley Coupling in a van Der Waals Ferroelectric Halide Perovskite with Persistent Spin Helix. *Nat. Photonics* **2022**, *16* (7), 529−537.
(39) Walser, M. P.; Reichl, C.; Wegscheider, W.; Salis, G. Direct Mapping of the Formation of a Persistent Spin Helix. *Nat. Phys.* **2012**, *8* (10), 757−762.
(40) Abdelwahab, I.; Kumar, D.; Bian, T.; Zheng, H.; Gao, H.; Hu, F.; McClelland, A.; Leng, K.; Wilson, W. L.; Yin, J.; Yang, H.; Loh, K. P. Two-Dimensional Chiral Perovskites with Large Spin Hall Angle and Collinear Spin Hall Conductivity. *Science* **2024**, *385* (6706), 311−317.
(41) Valenzuela, S. O.; Tinkham, M. Direct Electronic Measurement of the Spin Hall Effect. *Nature* **2006**, *442* (7099), 176−179.
(42) Tian, J.; Miotkowski, I.; Hong, S.; Chen, Y. P. Electrical Injection and Detection of Spin- Polarized Currents in Topological Insulator Bi2Te2Se. *Sci. Rep.* **2015**, *5* (1), 14293.
(43) Chen, H.-T.; Taylor, A. J.; Yu, N. A Review of Metasurfaces: Physics and Applications. *Rep. Prog. Phys.* **2016**, *79* (7), 076401.
(44) Tian, J.; Adamo, G.; Liu, H.; Klein, M.; Han, S.; Liu, H.; Soci, C. Optical Rashba Effect in a Light-Emitting Perovskite Metasurface. *Adv. Mater.* **2022**, *34* (12), 2109157.
(45) Long, G.; Adamo, G.; Tian, J.; Klein, M.; Krishnamoorthy, H. N. S.; Feltri, E.; Wang, H.; Soci, C. Perovskite Metasurfaces with Large Superstructural Chirality. *Nat. Commun.* **2022**, *13* (1), 1551.
(46) Jin, B.; Lu, Y.; Sun, J.; Sun, X.; Wen, L.; Zhang, Q.; Zhao, D.; Qiu, M. Cryogenic Electron- Beam Writing for Perovskite Metasurface. *Nano Lett.* **2024**, *24* (18), 5610−5617.
(47) Yumoto, G.; Harata, F.; Nakamura, T.; Wakamiya, A.; Kanemitsu, Y. Electrically Switchable Chiral Nonlinear Optics in an Achiral Ferroelectric 2D van Der Waals Halide Perovskite. *Sci. Adv.* **2024**, *10* (46), No. eadq5521.

https://doi.org/10.1021/acs.chemmater.5c01042
Chem. Mater. XXXX, XXX, XXX−XXX